Formation of corrosion pockets in FeNiCrAl at high temperatures investigated by 3D FIB-SEM tomography

(article starts on next page)

ARTICLE

Formation of corrosion pockets in FeNiCrAl at high temperatures investigated by 3D FIB-SEM tomography

Katrin Jahns[1] (ORCID) | **Ulrich Krupp[2]** | **Gustav Sundell[3]** | **Christine Geers[4]**

[1]Institute of Materials Design and Structural Integrity, University of Applied Sciences Osnabrück, Osnabrück, Germany

[2]Steel Institute IEHK, RWTH Aachen University, Aachen, Germany

[3]Vitroprobe Analytics AB, Gothenburg, Sweden

[4]Environmental Inorganic Chemistry, Chalmers University of Technology, Gothenburg, Sweden

Correspondence

Katrin Jahns, Institute of Materials Design and Structural Integrity, University of Applied Sciences Osnabrück, Albrechtstraße 30, 49076 Osnabrück, Germany.
Email: k.jahns@hs-osnabrueck.de

Abstract

A recently published study of high temperature nitridation of iron chromium aluminum alloys (FeCrAl) at 900°C in N_2–H_2 has redundantly shown the formation of locally confined corrosion pockets reaching several microns into the alloy. These nitrided pockets form underneath chromia islands laterally surrounded by the otherwise protective alumina scale. Chromia renders a nitrogen-permeable defect under the given conditions and the presence of aluminum in the alloy. In light of these findings on FeCrAl, a focused ion beam–scanning electron microscope tomography study has been undertaken on an equally nitrided FeNiCrAl sample to characterize its nitridation corrosion features chemically and morphologically. The alloy is strengthened by a high number of chromium carbide precipitates, which are also preferential chromia formation sites. Besides the confirmation of the complete encapsulation of the corrosion pocket from the alloy by a closed and dense aluminum nitride rim, very large voids have been found in the said pockets. Furthermore, metallic particles comprising nickel and iron are deposited on top of the outer oxide scale above such void regions.

KEYWORDS

FeNiCrAl, FIB-SEM tomography, nitridation, void formation

1 | INTRODUCTION

High-temperature alloys are designed to maintain sufficiently high mechanical strength at elevated temperatures and to resist rapid corrosion. Long-term corrosion resistance can be achieved by separating the corrosive gas from the metal via a slowly growing oxide scale, that is, chromia, alumina and/or silica. Alumina-forming alloys are an important group of high-temperature alloys due to the very high thermal and chemical stability of aluminum oxide, specifically α-alumina, which makes these alloys suitable for very high temperature applications

exceeding 900°C and within aggressive environments. Demanding conditions also include environments with small quantities of oxygen, in our case as low as 10^{-23} bar, which must be sufficient to create and stabilize the desired passive layer.

In an earlier work,[1] nitridation of a FeCrAl alloy Kanthal APMT™ was described after exposure to a mixture of 95% N_2, 5% H_2, and impurity levels of water vapor at 900°C. Herein, the corrosion front was either defined by a slow-growing alumina scale on top of the material or by local nitridation attack underneath a nonprotective chromia scale creating an inner aluminum nitride rim. Local nitridation

attack comprises within small areas of several cubic micrometers that are oversaturated with nitrogen. These areas are encapsuled by a nitride rim toward the bulk alloy and by chromia toward the gaseous environment; they are in the following referred to as "pockets." Inside such a pocket, aluminum and chromium are completely nitridated within an almost pure iron matrix. Beyond the AlN rim, the alloy matrix has been apparently unaffected, which is not surprising since AlN has proven to be an efficient barrier against carbon.[2]

The FeNiCrAl alloy studied here is strengthened by $Cr_{23}C_6$ precipitates. The evolution of such carbides in high-temperature oxidizing conditions has been studied extensively for nickel base alloys[3–5] and austenitic alloys,[6] where it was found that the growth of an oxide scale during high-temperature oxidation depletes the subsurface region of chromium, which causes the dissolution of chromium carbide particles. While chromium is oxidized, the released carbon diffuses deeper into the alloy toward regions with higher chromium activity. Internal nitridation of chromium carbides can be regarded analogously to the chromium consumption by internal oxidation. In both cases, the carbon activity increases. The transformation of carbide precipitates in steels by nitrogen was already observed for inner liners of Haber–Bosch ammonia synthesis vessels at much lower temperatures around 432°C.[7] Here, released carbon originating from the transformed carbides effuses from the steel and can react with diffusing hydrogen to form methane.[7] However, the formation of enclosed corrosion pockets in the case of FeCrAl nitridation,[1] and as shown in this study for FeNiCrAl, eventually does not allow back diffusion of carbon deeper into the alloy as described in References [3–6]. Entrapping of carbon in a small corrosion volume allows for alternative reaction paths, which are discussed in this paper, achieving at an emerging mechanistic understanding for the corrosion phenomena found, that is, correlated void formation in corrosion pockets in conjunction with metal extrusions.

2 | EXPERIMENTAL PROCEDURE

In this study, a FeNiCrAl model alloy was exposed to a mixture of 95% N_2 and 5% H_2 containing part per millions of water vapor as impurity at 900°C, by which a heat treatment environment encountered in, for example, steel production and sintering, is simulated. The nominal chemical composition of the investigated FeNiCrAl model alloy, based on the composition of Nikrothal PM58™, is given in Table 1. It has to be mentioned that a relatively high C content of 0.15 wt% is present in the investigated alloy leading to a high number of $Cr_{23}C_6$ precipitates. The FeNiCrAl material was cut into

$15 \times 15 \times 2$ mm^3 coupons, which were ground and polished to a mirror-like 1-μm diamond paste finish. After thorough rinsing in water as well as ultrasonical cleaning in ethanol and acetone baths, the samples have been mounted on an alumina sample holder and placed in a horizontal furnace tube. The experiment was started by purging the furnace tube with the N_2–5% H_2 gas mixture for at least 8 hr to remove traces of air to a minimum. After rapid heating to target temperature in 30 min, the samples were kept at 900°C for 168 hr and cooled down slowly within 5 hr in the furnace afterward. The gas flow was 100 ml/min corresponding to a net average gas flow speed of 6.3 cm/min in the tube.

Trace amounts of oxygen (about 15 ppm) were measured in the nitrogen gas by means of a zirconia oxygen sensor, Rapidox 2100, at 700°C operational temperature. Equilibrating the residual oxygen with hydrogen at 900°C results into a complete conversion to steam and in an oxygen activity of 10^{-23} (calculated by FactSage[8]), which is higher than the Cr_2O_3 dissociation pressure at equilibrium 4.4×10^{-24} bar.[9]

Microstructural characterization was carried out by means of scanning electron microscopy (SEM; Zeiss Auriga FEG and FEI Quanta 200 FEG) in combination with energy-dispersive X-ray spectroscopy (EDS) and focused ion beam (FIB) milling. The FIB-SEM tomography was performed using the Zeiss SmartSEM software. To perform a 3D tomography, the observed area was layered, FIB cuts were performed for every layer and respective SEM images recorded. The resembling step width of two layers was set to a value of 10 nm. After performance of the 3D tomography, a 3D reconstruction was executed using the software Dragonfly Pro 2.0. Furthermore, EDS measurements on the surface achieved by FIB were performed using an Oxford Instruments silicon drift detector (X-Max, 80 mm^2) in combination with the AZTEC software. An automatic correction factor within the AZTEC software is considered to account for the tilt of the sample by 54° necessary for the FIB cut.

3 | EXPERIMENTAL AND CALCULATION RESULTS

3.1 | Formation of a corroded pocket

Kanthal APMT™ contains only 0.08 wt% of carbon[1] compared with 0.15 wt% in Nikrothal PM58™. Inherent

TABLE 1 Nominal chemical composition of the FeNiCrAl model alloy

Wt%	Ni	Cr	Al	Fe	C	Others
Nominal	Bal.	17–19	4–5	18–20	0.15	Traces

excess carbon in the FeNiCrAl alloy causes chromium carbide precipitation creating the characteristic microstructure of this alloy. An overview image of a representative surface area taken before exposure is shown in Figure 1a. $Cr_{23}C_6$ in proximity to the alloy surface act as chromia nucleation sites due to their aluminum deficiency. The ternary phase diagram of Cr–C–Al at 900°C in Figure 1b (calculated with the ThermoCalc TCFE8 database[10]) shows no solubility of aluminum in chromium carbides. Thus, locally, the $Cr_{23}C_6$ precipitates at the alloy surface nucleates Cr_2O_3 instead of alumina. This hypothesis is supported by EDS investigations of samples with marked areas before and after heat treatment, see Figures 1c and 1d, respectively. The nitridation attack was tracked in a $10 \times 10\,\mu m^2$ region by performing a focused EDS mapping before and after the exposure and marking the respective areas with FIB. Before exposure, a Cr carbide was present in the marked area. After exposure, the Cr carbide had dissolved and the formation of Cr_2O_3 instead was visible. Consequently, the number of formed chromia domains with underlying nitridation pockets had increased with the number of chromium carbide particles comparing FeNiCrAl Nikrothal PM58™ alloy and FeCrAl Kanthal APMT™.[1]

Chromium oxide has been identified by experiment and ab initio calculations as a nitrogen-permeable phase during the nitridation of FeCrAl Kanthal APMT™.[1] This has been confirmed in this study for the FeNiCrAl alloy Nikrothal PM58™, by finding consistently nitrided pockets underneath every chromia domain. After 168 hr at 900°C in N_2-5% H_2 (ppm H_2O) nitridation of the FeNiCrAl presents as a local corrosion feature with the shape of approximately half spherical pockets. Figure 2 shows a cross-sectioned pocket prepared by broad ion beam in electron backscatter contrast. Point analysis by EDS was used to gain phase composition information. The diameter range of these pockets is between 5 and $15\,\mu m$, significantly smaller than those reported for Kanthal APMT™[1] and following features of the fine-grained microstructure. The corrosion front comprises of a closed aluminum nitride rim acting as effective diffusion barrier for further oxidant diffusion into the alloy matrix.[2]

Within the pocket, all aluminum and chromium had reacted to AlN, CrN or Cr_2N, only nickel and iron were detected in solution of the residual alloy. $Cr_{23}C_6$ could no longer be found within the pocket.

3.2 | Investigation of corroded pockets by FIB-SEM tomography

Figure 3 shows a back-scattered electron image of a corroded pocket taken during an FIB-SEM tomography with the parameters mentioned above and the resembling 3D reconstruction carried out by Dragonfly Pro 2.0. Besides the expected rim delimiting the pocket and an oxide scale with formation of whiskers, the presence of large porosities becomes evident (see Figure 3a). Tilting of the sample by ±5° reveals that the porosity does not vanish and hence, an electron-optical artefact due to the FIB-SEM treatment as described in Cruchley et al.[11] can ruled out. After evaluation of all images taken during the tomography, the 3D reconstruction shown in Figure 3b represents one complete corroded pocket. The 3D reconstruction in combination with the SEM micrographs conducted from the tomography reveal that the pocket is densely closed by an AlN rim. Furthermore, discovering large voids and reconstruction of their position in the corrosion volume in 3D as shown in Figure 3c renders them rather disconnected from the oxide scale. Multiple repetitions of the tomography on numerous corroded pockets support the conclusion that the situation shown in Figure 3 is no individual case and void formation occurs within all corroded pockets but never beyond the aluminum nitride rim. Thus, mechanistic understanding concerning pocket formation due to internal nitridation presented and described earlier[1] needs to be revised or extended.

The results of EDS measurements performed on top views and FIB cuts of the sample after nitridation are shown in Figure 4. The magenta areas represent the Al_2O_3 scale covering the major fraction of the sample surface, whereas yellow areas indicate Cr_2O_3 domains, where corroded pockets are located underneath. Furthermore, unreacted substrate material extrusions consisting of Fe and Ni as shown in blue may be detected outside of the oxide scale on top of the sample, see Figures 4a and 4c, respectively. Figure 4a,b show top views on the chromia caps of the corroded pocket with Fe and Ni extrusions being located on top, favorably at the end of elongated ejections acting as channels consisting of chromia. Figure 4c shows both, a SEM image of an FIB cut and the resembling EDS measurement, where both the occurrence of Fe and Ni extrusions and a channel toward these is visible. Probably, Fe and Ni are driven through the channels toward the surface. On top of the chromia cap, Fe and Ni are neither nitrided nor oxidized. As described before, void formation within the nitrided pocket has been observed, in some cases located underneath the extrusions, but not necessarily in contact with the oxide scale. In some cases, these voids were found several micrometers away from the oxide scale, deep inside the pocket.
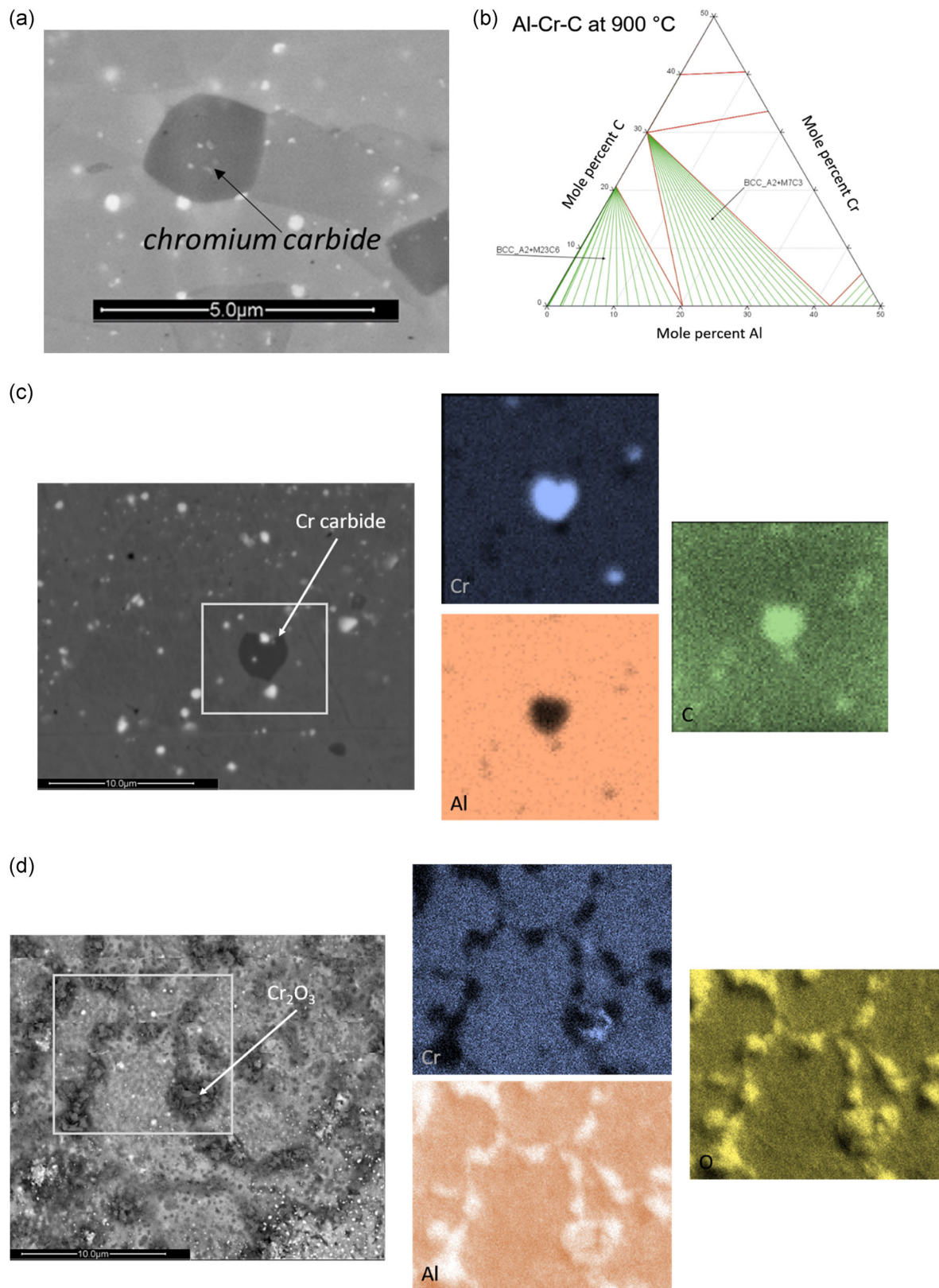
FIGURE 1 (a) Back-scattered electron image of the surface of the uncorroded sample with a representative chromium carbide; (b) ternary Al–Cr–C phase diagram calculated with ThermoCalc,[7] (c) energy-dispersive X-ray spectroscopy (EDS) mapping of a marked area with a Cr carbide before exposure, (d) EDS mapping of the same marked area with Cr_2O_3 formation at the original position of the Cr carbide after exposure [Color figure can be viewed at wileyonlinelibrary.com]
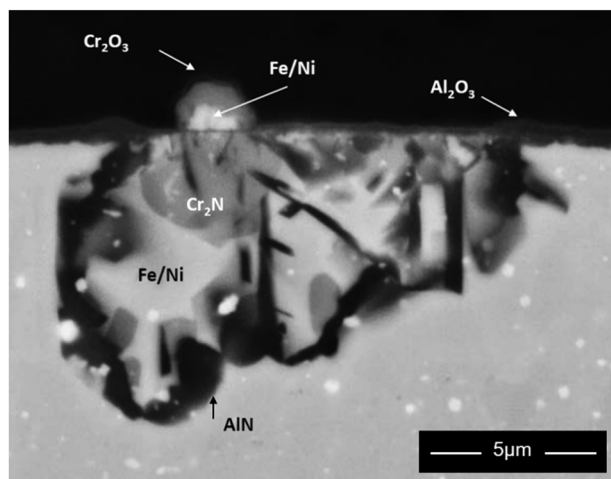
FIGURE 2 Back-scattered electron image of the cross-section of a corroded pocket with information on the formed phases taken by energy-dispersive X-ray spectroscopy point analysis

4 | DISCUSSION

4.1 | Formulation of a mechanism for the formation of corrosion pockets

The nitridation pockets formed in FeNiCrAl have been shown by FIB-SEM tomography (Figure 3) to be completely sealed from the alloy substrate by a dense aluminum nitride rim. This has been proven by the tomographic analysis as well as implicitly by the absence of nitride precipitates outside the pocket, see also the studies presented in Geers et al.[1] Thus, only reactions within the pocket, originating from a chromium carbide, shall be focused on. In the following, the evolution of such a pocket is dissected into the partial steps oxidation and nitridation. The sequence is illustrated in Figure 5.

Step 1: The nitriding environment at high temperature is in contact with the $Cr_{23}C_6$-rich FeNiCrAl alloy at
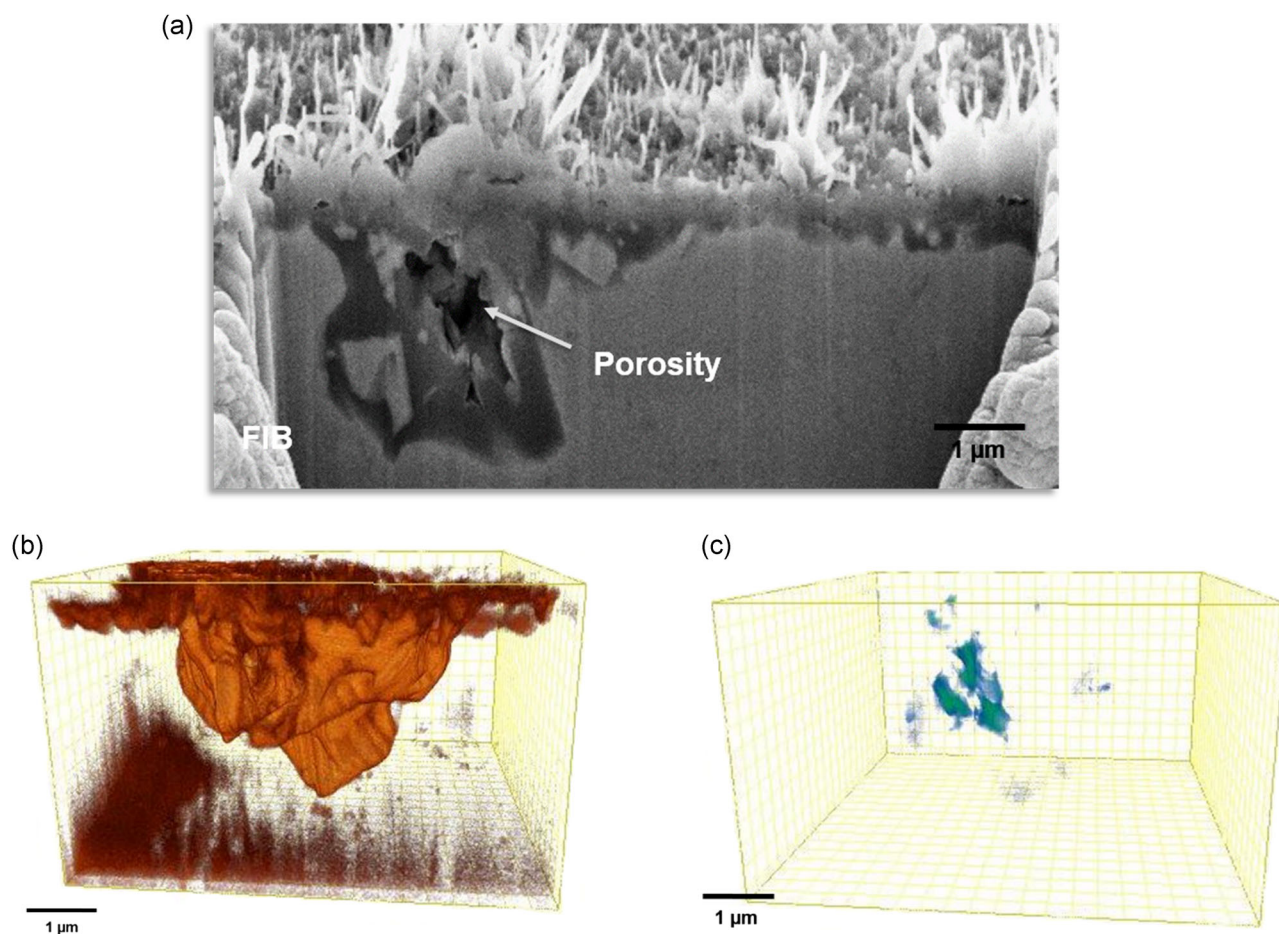

FIGURE 3 (a) Back-scattered electron image of the cross-section of a corroded pocket taken during a focused ion beam–scanning electron microscope (FIB-SEM) tomography showing the existence of porosity. 3D reconstruction by means of Dragonfly Pro 2.0 of the FIB-SEM tomography partly shown in (a); (b) presentation of the whole pocket in orange, (c) uncovering of the porosities (blue) inside the pocket [Color figure can be viewed at wileyonlinelibrary.com]

FIGURE 4 Energy-dispersive X-ray spectroscopy (EDS) mappings of a corroded pocket and visualization of the base material (Fe, Ni shown in blue) and channels: (a) top view on the surface of the sample, (b) scanning electron microscopy image of the chromia cap of a corroded pocket with visible extrusion of base material (Fe, Ni) at the ending of channels, and (c) focused ion beam (FIB) section with focus on a distinct pocket with porosity, Fe and Ni extrusions, and visualization of channels [Color figure can be viewed at wileyonlinelibrary.com]
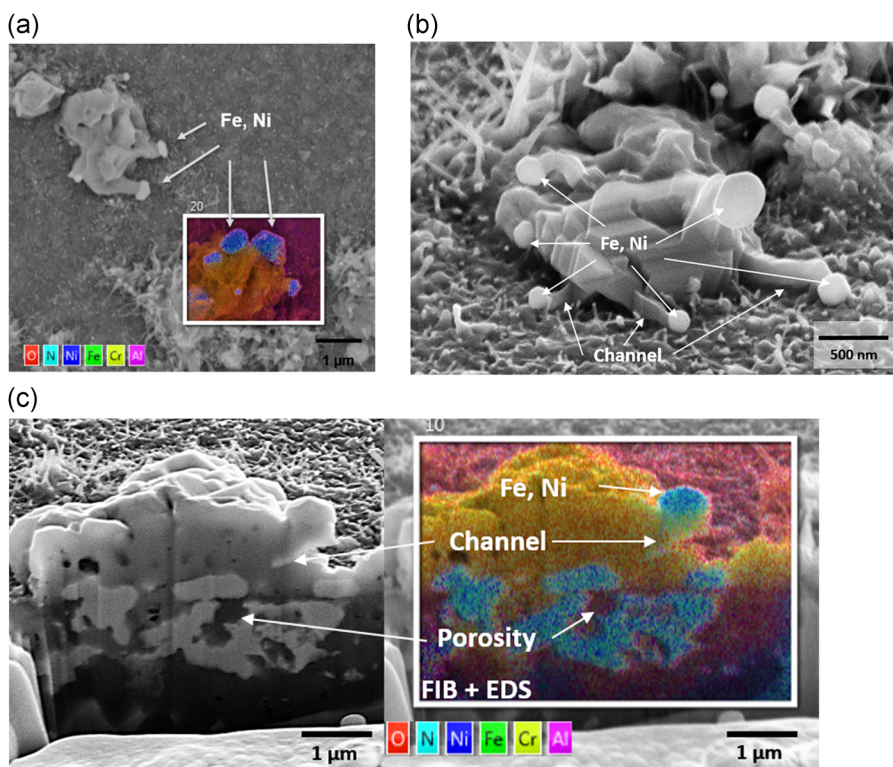
elevated temperature. The carbide phase contains no aluminum, compare Figure 1b.

Step 2: The impurity water vapor in the environment nucleates oxide films on the surface of the sample, alumina on the alloy substrate, and chromia on chromium carbide particles. The necessary Cr is originating from the chromium carbides that transform in the N_2–H_2 atmosphere and releases carbon, see also Heuser et al.[7] The inwards growing oxide scale releases continuously hydrogen into the alloy, see also Mortazavi et al.[12]

Step 3: Cr_2O_3 domains permeate nitrogen and enable internal nitridation.[1] Aluminum in the substrate reacts with nitrogen leading to the formation of the sealing aluminum nitride rim, compare Figures 2 and 4b.

Step 4: After all, aluminum within the corrosion pocket is consumed by nitrogen, nitridation continues converting chromium from the matrix and the $Cr_{23}C_6$ to Cr_2N subsequently releasing carbon analogously to the internal oxidation reaction described by Petkovic-Luton and Ramanarayanan.[13] Carbon originating from the chromium carbides remains inside the pocket, incapable to dissolve into the metal due to the closed ring of AlN formed in Step 3.

All in all, the corroded volume comprises of a sealed capsule containing iron and nickel oversaturated with carbon, aluminum, and chromium nitride precipitates and a terminating aluminum nitride rim toward the alloy as well as an oxide scale toward the gas environment.
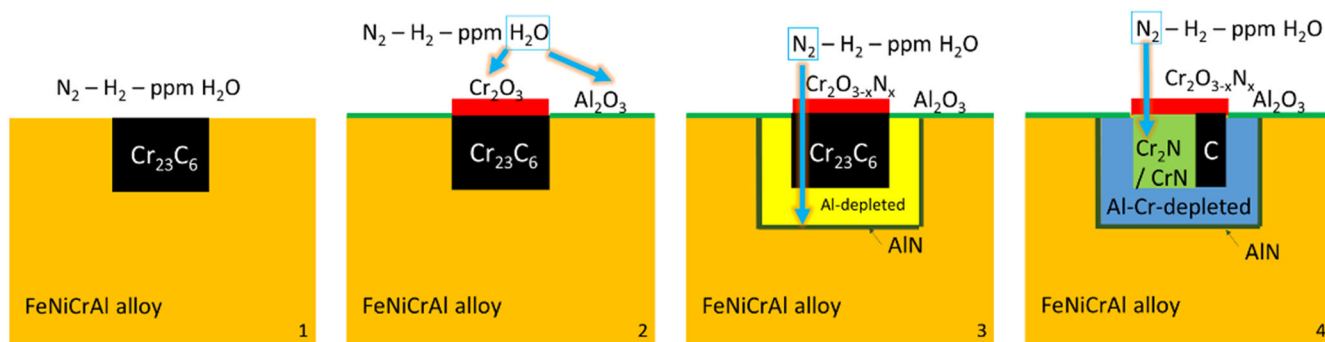

FIGURE 5 Schematic representation of the stepwise mechanism for the concurrent formation of corrosion pockets and porosities [Color figure can be viewed at wileyonlinelibrary.com]

In addition to these features originating from the four steps of corrosion, large channels and extrusions are observed.

4.2 | Discussion of void formation in combination with metal extrusions

The formation of voids in combination with metal extrusions at the surface of the sample (see Figure 4) needs to be discussed more in detail. In the following, mechanisms that have been discarded for the present corrosion phenomenon are discussed in short, (a) formation of Kirkendall porosity[14] and (b) occurrence of surface protrusions.[15,16] Kirkendall porosity,[14] as origin of complex-shaped voids during corrosion and formed due to variations in the intrinsic diffusivities, are feasible as initial origin of pores during the chromia formation (Figure 5; Step 2). This type of porosity can serve as a volume reservoir which can be populated either by alloy or gas species in the progressing corrosion process. Instead of filling up the available porosity volume fraction, the unreacted alloy species iron and nickel were found in the form of extrusions at the end of elongated ejections on top of the chromia, which was not reported in the context of Kirkendall porosity yet. Thus, the occurrence of Kirkendall porosity as origin of the observed effect is not unambiguous.

Furthermore, the formation of protrusions during nitridation of binary, ternary, and quaternary Ni–Cr–Ti–Al nickel base model alloys was observed in References [15,16]. Internal nitridation kinetics of TiN and AlN were reported to increase with increasing chromium content and decrease with increasing content of the nitride-forming alloying elements. The large volume change, resulting from the difference in the specific volumes of the solute in the alloy, and the corresponding nitride compound produce a stress gradient between the stress-free surface and the internal nitridation front. Microstructural examinations and theoretical calculations showed that an outward diffusion flux of metallic elements compensates the internal nitridation-induced volume increase and relieves the internal stresses within the precipitation zone. As a consequence, all specimens exhibit substrate protrusions on the surface, formed during the internal nitridation process. The volume of these protrusions is very similar to the total volume increase caused by the internal nitridation process.[15,16] In framework of this study, the question arises whether the substrate extrusions at the surface as shown in Figure 4 represent actually protrusions due to internal stresses within the nitridation pocket. However, the experimental observations described in this study show two major

deviations from the explanations in References [15,16]: First, for the occurrence of substrate protrusions caused by internal stresses, no pore formation is detectable. In addition, the substrate extrusions presented in this study are restricted to areas affiliated with nitridation pockets and the concurrent formation of pores. Second, the protrusions reported in References [15,16] are directly located at the surface of the sample, thus still in contact with the base material feeding the protrusions, whereby the substrate extrusions reported in this study are occurring above a chromia scale at the end of elongated channels, see Figure 4b, without any junction to the substrate and only in the presence of a pore underneath the scale. In regions with solely alumina scale formation, no extrusions were found.

However, the origin of the voids in combination with unreacted alloy species iron and nickel on top of the surface could not be clarified by these approaches. A speculative hypothesis, based on carbon release from chromium carbides and hydrogen penetration as described in Heuser et al.[7] for lower temperatures, is that a gas pressure build-up within the corrosion pockets leads to void formation and metal extrusions at the surface of the sample. In the following, the hypothesis is further explained.

Gas evolution, more specifically methane evolution in an alloy, was reported by Heuser et al. for Haber–Bosch vessels at lower temperatures (<500°C),[7] causing severe weakening of the steel integrity. At higher temperatures, the solubility of carbon into the alloy is higher as its diffusivity, allowing it to diffuse away from the reaction front when, for example, chromium is consumed by oxidation.

Local nitridation formed in our case, however, a corroded pocket. The carbon released during nitridation of a chromium carbide particle is not allowed to diffuse deeper into the alloy due to the entrapment by the closed AlN rim (see Figures 2 and 4b). Studies where the relative stabilities of the different nitrides were discussed to demonstrate the presence of a closed AlN rim were already presented by Geers et al.[1] in a previous work. Aluminum nitride offers a factor two higher stability compared with the most stable chromium nitride, CrN, at 900°C. Thus, the corrosion pocket is separated from the substrate material by the AlN rim, forming a confined volume before nitridation of chromium species can occur.

The internal nitridation of chromium carbide particles to chromium nitride follows the same path as reported for carbon release from $Cr_{23}C_6$ during internal oxidation.[13]

Within the metal, dissolved nitrogen and hydrogen are possible reactants together with the released and oversaturated carbon in the small and confined corrosion

pocket. Considering this interior chemistry, a hypothetic mechanism for the formation of voids might be the reaction of carbon and hydrogen to methane, which would be endotherm if the reaction happens in gas phase at 900°C. Hereby, however, associated corrosion processes are already dissociating the strong bonds of N_2 and H_2[1,12] before meeting the chromium carbide, thus providing a strong exothermic shift.

The key is the location of the reaction between dissolved species within the internal nitridation pocket rather than in gas phase or at the oxide/gas interphase. Considering the solid/gas conversion processes as internal processes in the alloy, a consequential pressure build-up occurs, leading to the formation of large voids (see Figure 3c). Substrate material Fe and Ni as the remaining unreacted alloy species in the nitridation pocket are pressed outward, leading to the formation of channels and metal extrusions on the surface (see Figure 4).

These channels are visible in a top view together with extrusions, see arrows in Figure 4b,c, and could neither be explained by Kirkendall diffusion nor protrusion formation as described in References [15,16]. These experimental observations shown in Figure 4 coupling large voids in nitride pockets and metal extrusion through the outer oxide scale support the hypothesis of a substantial pressure build-up by evolution of a gaseous phase such as methane. Since the formation of large voids within corrosion pockets in combination with metallic extrusions on top of the pockets have not been reported before, further investigations are required to support the hypothesis outlined above, and the classical approaches have to be reconsidered.

5 | CONCLUSION

In this study, the formation of corrosion pockets by 3D FIB-SEM tomography is described. Nitridation at 900°C occurs underneath well-defined Cr_2O_3 domains while the major area fraction is covered by a protective Al_2O_3 scale. Internal nitridation of Nikrothal PM58™ resembles small pockets. In this study, we could show that these pockets are completely sealed toward the bulk alloy by a dense AlN rim. As not yet reported for internal nitridation, inside the pocket, the formation of large voids was observed with concurrent occurrence of substrate extrusions of unreacted alloy species on top of the chromia domain at the gas/oxide interface. Based on EDS analyses and FIB-SEM tomography, the emerging mechanistic understanding can be summarized as a four-step mechanism presented in the discussion:

Step 1: The nitriding environment at high temperature is in contact with the $Cr_{23}C_6$-rich FeNiCrAl alloy at elevated temperature.

Step 2: The impurity water vapor in the environment nucleates oxide films on the surface of the sample, alumina on the alloy substrate and chromia on chromium carbide particles. Hydrogen is released into the alloys.

Step 3: Cr_2O_3 domains permeate nitrogen and enable internal nitridation. Aluminum in the substrate reacts with nitrogen leading to the formation of the sealing aluminum nitride rim.

Step 4: Aluminum within the corrosion pocket is consumed by nitrogen, nitridation continues converting chromium from the matrix and the $Cr_{23}C_6$ to Cr_2N subsequently releasing carbon. Carbon originating from the chromium carbides remains inside the confinedvolume of the corrosion pocket.

ORCID

Katrin Jahns https://orcid.org/0000-0001-6492-6169

REFERENCES

[1] C. Geers, V. Babic, N. Mortazavi, M. Halvarsson, B. Jönsson, L.-G. Johansson, I. Panas, J.-E. Svensson, *Oxid. Met.* **2017**, *87*, 321.

[2] V. P. Godbole, K. Jagannadham, J. Narayan, *Appl. Phys. Let.* **1995**, *67*, 1322.

[3] A. Chyrkin, P. Huczkowski, V. Shemet, L. Singheiser, W. J. Quadakkers, *Oxid. Met.* **2011**, *75*, 143.

[4] R. Pillai, H. Ackermann, H. Hattendorf, S. Richter, *Corros. Sci.* **2013**, *75*, 28.

[5] A. Chyrkin, R. Pillai, H. Ackermann, H. Hattendorf, S. Richter, W. Nowak, S. Grüner, W. J. Quadakkers, *Corros. Sci.* **2015**, *96*, 32.

[6] K. Ledjeff, A. Rahmel, M. Schorr, *Mater. Corros.* **1979**, *30*, 767.

[7] A. Heuser, G. H. Wagner, G. Heinke, V. Číhal, *Steel Res.* **1993**, *64*, 454.

[8] C. W. Bale, E. Bélisle, P. Chartrand, S. A. Decterov, G. Eriksson, A. E. Gheribi, K. Hack, I. H. Jung, Y. B. Kang, J. Melançon, A. D. Pelton, S. Petersen, C. Robelin, J. Sangster, M.-A. Van Ende, *Calphad* **2016**, *54*, 35.

[9] J. T. Ellingham, *J. Soc. Chem. Ind.* **1944**, *63*, 125.

[10] J. O. Andersson, T. Helander, L. Höglund, P. F. Shi, B. Sundman, *Calphad* **2002**, *26*, 273.

[11] S. Cruchley, J. F. Sun, M. P. Taylor, H. E. Evans, P. Bowen, J. Sumner, J. R. Nicholls, N. J. Simms, B. A. Shollock, R. J. Chater, B. J. Foss, M. C. Hardy, S. Stekovic, *Mater. High Temp.* **2014**, *31*, 27.

[12] N. Mortazavi, C. Geers, M. Esmaily, V. Babic, M. Sattari, K. Lindgren, P. Malmberg, B. Jönsson, M. Halvarsson,

J. E. Svensson, I. Panas, L. G. Johansson, *Nat. Mater.* **2018**, *17*, 610.

[13] R. Petkovic-Luton, T. A. Ramanarayanan, *Oxid. Met.* **1990**, *34*, 381.

[14] H. Mehrer, *Diffusion in Solids*, Springer, Heidelberg **2007**.

[15] U. Krupp, H. J. Christ, *Oxid. Met.* **1999**, *52*, 277.

[16] S. Y. Chang, U. Krupp, H. J. Christ, *Mater. Sci. Eng. A* **2001**, *301*, 196.